Journal of Alloys and Compounds 509 (2011) 5866–5872

Contents lists available at ScienceDirect

Journal of Alloys and Compounds

journal homepage: www.elsevier.com/locate/jallcom

Influence of withdrawal rate on the microstructure of Ni-base single-crystal superalloys containing Re and Ru

Gang Liu [a], Lin Liu [a,*], Cheng Ai [b], Bingming Ge [a], Jun Zhang [a], Hengzhi Fu [a]

[a] State Key Laboratory of Solidification Processing, Northwestern Polytechnical University, Xi'an, 710072, China
[b] Material Science and Engineering School, BeiHang University, Beijing, 100083, China

ARTICLE INFO

Article history:
Received 11 November 2010
Received in revised form 23 February 2011
Accepted 25 February 2011
Available online 5 March 2011

Keywords:
High-temperature alloys
Crystal growth
Microstructure
Scanning electron microscopy

ABSTRACT

The influence of elevated withdrawal rate on the microstructure and segregation behavior of Ni-base single-crystal superalloys containing Re and Ru is investigated. The experimental superalloys are processed under a high thermal gradient of approximately 250 K/cm and withdrawal rates between 10 and 500 μm/s. With increasing withdrawal rate, the dendritic structures and γ′ precipitates in as-cast microstructures are apparently refined. Electron-probe microanalyzer (EPMA) results indicate that the degree of segregation for the constituent elements (e.g. Al, Ta, W, Re etc.) increases initially and then decreases with increasing withdrawal rate. In addition, the Re and Ru additions obviously increase the amounts of γ–γ′ eutectic and the tendency of segregation for Al and Ta.

© 2011 Elsevier B.V. All rights reserved.

1. Introduction

Due to the excellent high temperature mechanical and thermal properties, Ni-base single-crystal superalloys have been widely used for manufacturing the turbine blades for aero-engines and industry gas turbine (IGT) [1–3]. To improve the high temperature performance, the total amount of refractory elements addition in modern Ni-base superalloys is gradually increased. However, the addition of refractory elements (i.e. Re and W) also leads to many problems, such as: (1) severe segregation [4,5]; (2) increasing tendency of grain defects formation [6]; (3) complicated solution heat treatments [7]; (4) increasing tendency of detrimental topologically-closed-packed (TCP) phases formation [8]. To overcome above-mentioned problems, approximately 2–6 wt.% Ru has been added to the newly developed single-crystal superalloys.

Nowadays, the "high rate solidification (HRS)" technique is the prevalent manufacturing process for turbine blades. Unfortunately, because of its relative low thermal gradient (<100 K/cm), the withdrawal rate must be ranged from 3 to 6 mm/min to prevent the formation of equiaxed grains. In addition, HRS technique is difficult to be used for casting the complicated large IGT blades for numerous problems relating to low growth rate and casting defects. It has been proved to be an efficient way to suppress the grain defects formation by increasing the thermal gradient during directional solidification. Therefore, many new technologies, such as gas cooling casting (GCC) [9], fluidized-bed quenching (FBQ) [10], and liquid metal cooling (LMC) [11,12] processes have been developed to increase the thermal gradient during solidification. The thermal gradient of LMC process is 2–4 times greater than that of HRS method, which results in the reduction of dendrite arm spacing and segregation of alloying elements. However, still few researches focus on the microstructure of Re- and Ru-containing single-crystal superalloys under high thermal gradient directional solidification.

In this investigation, four single-crystal superalloys with varied contents of Re and Ru are prepared. The influence of elevated withdrawal rate on the segregation ratios of the constituent elements is investigated. The corresponding as-cast microstructures under high thermal gradient directional solidification are also discussed.

2. Materials and experimental procedures

The chemical compositions of the experimental alloys used in this investigation are presented in Table 1. The increasing contents of Re and Ru are added at the expense of Ni, but other constituent elements almost keep constant. Due to the limited content of Hf, its effects can be neglected in this investigation.

Single-crystal bars (4 mm in diameter and 70 mm in length) were produced with the bottom-seeding technique by using a modified directional solidification apparatus described elsewhere [13]. A high thermal gradient is obtained in this research, which can be attributed to the introductions of dual resistance heating zones melting, carefully designed heat baffles and low melting coolant (Ga–In–Sn liquid metals). The temperature gradient was measured by W/Re thermocouples that were placed near the outside surface of the alumina crucible. One of the thermocouples was placed about 10 mm from the bottom of the sample, where it was close to the solid–liquid interface. The other thermocouple was placed approximately 20 mm from the bottom of the sample. The temperature gradient close to the liquid/solid interface was measured to be approximately 250 K/cm.

* Corresponding author. Tel.: +86 29 8849 2227; fax: +86 29 8849 2227.
E-mail address: linliu@nwpu.edu.cn (L. Liu).

0925-8388/$ – see front matter © 2011 Elsevier B.V. All rights reserved.
doi:10.1016/j.jallcom.2011.02.156

Table 1
Compositions of the experimental single crystal alloys used in this investigation (wt.%).

Alloys	Cr	Co	Mo	W	Al	Ta	Hf	Re	Ru	Ni
A	3.01	11.6	1.02	5.90	6.11	7.73	0.04	3.16	–	Bal.
B	3.18	12.1	1.01	5.95	6.05	7.95	0.08	4.00	–	Bal.
C	2.99	11.8	1.03	5.85	6.08	7.79	0.09	6.04	–	Bal.
D	2.93	11.7	1.03	6.01	5.98	7.84	0.06	6.20	3.03	Bal

Standard metallographic techniques were employed for the preparation of specimens. To reveal the microstructure, specimens were etched with a solution of HNO_3 (3 ml) – HF (6 ml) – $C_3H_8O_3$ (9 ml). The microstructure was observed with an optical microscopy (OM, Leica DM-4000 M) and a scanning electron microscopy (SEM, JEOL JSM-6040). The primary dendrite arm spacing (λ_1) was calculated by the area counting method on the transverse sections with the equation $\lambda_1 = (A/N)^{0.5}$, where A was the area of the region selected, N was the average number of primary dendrites in the area A. At least 30 regions in 3 specimens were measured for the data N. The secondary dendrite arm spacing (λ_2) was measured by SISC IASV8.0 analysis software in the longitudinal sections. At least 30 readings were taken for each sample and the value of λ_2 was their mean value.

To calculate the phase area fractions for the as-cast microstructure, the low-magnification SEM images were used in this investigation. The procedures for analyzing image were as follows: (1) adjusting the brightness and the contrast settings to clearly delineate the eutectic and dendritic regions; (2) setting the black and white threshold with the digital image analysis software SISC IAS V8.0; (3) distinguishing the phases with software; (4) manually filling the eutectic regions with color and calculating the phase fractions. At least 10 images under the same magnification were measured for each sample.

In order to study the segregation behavior of constituent elements, quantitative composition measurements were carried out on the as-cast specimen in as-polished condition using electro microprobe analyzer (EPMA) JXA-8100 equipped with wavelength dispersive X-ray spectroscopy (WDX). The instrument was operated at an accelerating voltage of 20 kV, a beam current of 100 nA and a spot size of 1 μm. At least 20 WDX point-scans were performed on the representative area for each alloy, 10 points within the dendrite core regions and 10 points within the interdendritic regions. Meanwhile, to qualitatively characterize the segregation behaviors of alloying elements, the energy dispersive spectrometer (EDX) area-scans were performed on the representative regions for the experimental alloys.

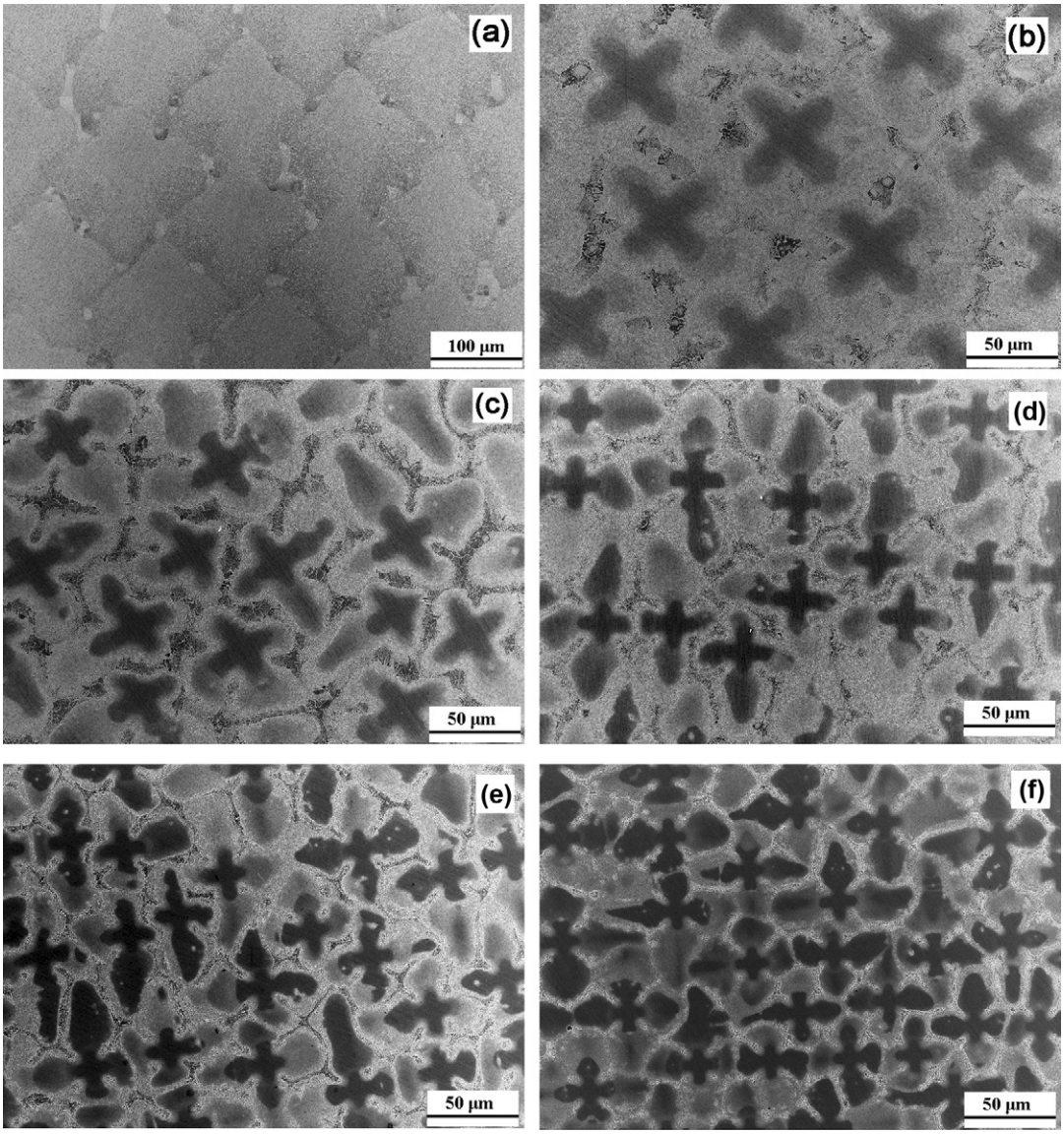

Fig. 1. Cross-sectional as-cast microstructures of alloy D at various withdrawal rates. (a) V = 10 μm/s; (b) V = 50 μm/s; (c) V = 100 μm/s; (d) V = 200 μm/s; (e) V = 300 μm/s; (f) V = 500 μm/s

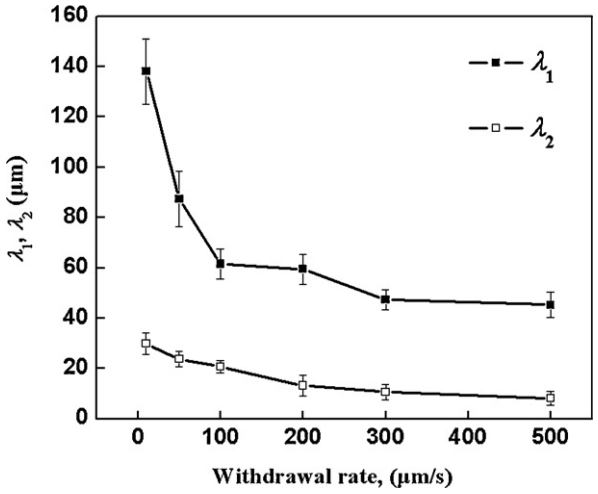

Fig. 2. Primary dendrite arm spacing (λ_1) and secondary dendrite arm spacing (λ_2) of alloy D at various withdrawal rates.

3. Results and discussion

3.1. Effects of withdrawal rate on the dendritic structures

Fig. 1 shows the transverse cross sections of the unidirectional solidified alloy D at different withdrawal rates: 10, 50, 100, 200, 300 and 500 μm/s. The typical dendritic structures with γ–γ′ eutectic in the interdendritic regions were obtained. With increasing withdrawal rates, the morphologies of as-cast microstructures change from cellular-dendrite (Fig. 1(a)) to coarse-dendrite (Fig. 1(b) and (c)) and then to fine-dendrite (Fig. 1(d)–(f)). The quantitative results of the primary dendrite arm spacing (λ_1) and secondary dendrite arm spacing (λ_2) are shown in Fig. 2. As well known, the value of λ_1 is a function of withdrawal rate (V) and thermal gradient (G) [14–16], as originally proposed by Hunt [17]:

$$\lambda_1 \propto G^{-1/2}V^{-1/4} \quad (1)$$

With increasing withdrawal rate, the dendritic structure is significantly refined. In our experiment, the value of λ_1 is only about 50 μm at the condition of G = 250 K/cm and V = 500 μm/s. Moreover, the value of λ_2 is related with the cooling rate ($G \times V$) [14]:

$$\lambda_2 \propto (G \times V)^{-1/3} \quad (2)$$

With increasing withdrawal rates up to 500 μm/s, the cooling rate increases to about 12.5 K/s, and the corresponding value of λ_2 is only about 8 μm.

Fig. 3(a) shows the longitudinal cross sections of the ⟨0 0 1⟩ orientated seed, which is produced with the HRS technique at the condition of V = 100 μm/s and G = 50 K/cm. Fig. 3(b) shows the quenched solid–liquid interface of alloy D at the same withdrawal rate in this research. Compared with the microstructure produced with HRS technique, the dendritic structure is significantly refined with high thermal gradient LMC technique. The λ_1 of alloy D is approximately 60 μm, which is one-sixth of the λ_1 (~370 μm) of the seed. The λ_1 is far away from the threshold (λ_1 about 320 μm) for freckle chains formation in the third generation single crystal SX-1 [6]. Therefore, it is an efficient way to suppress the grain defects formation with high thermal gradient LMC technique.

3.2. Effects of withdrawal rate on the γ–γ′ eutectic

The representative γ–γ′ eutectics of alloy D at different withdrawal rates are provided in Fig. 4. At the low withdrawal rate of 10 μm/s, the large blocky (region A) or rosette-like (region B) eutectic are obtained in the interdendritic regions, as shown in Fig. 4(a). The results of EDS area scans indicate that the blocky and rosette-like eutectic pools have the similar compositions (Table 2). The Al and Ta preferentially partition to the γ–γ′ eutectic, whereas Re, W, Co and Ru preferentially partition to the dendrite regions. With increasing withdrawal rate, the morphologies of eutectic gradually change from isolated blocky or rosette-like structures (Fig. 4(a)) to continuous strip-like structures (Fig. 4(b) and (c)). In addition, the size of eutectic significantly decreases with increasing withdrawal rate.

The eutectic fractions in as-cast alloys A, B, C and D at different withdrawal rates are calculated by the digital analysis software SISC IAS V8.0. The results of eutectic fractions are shown in Fig. 5. It indicates that the eutectic fractions increase initially and then decrease with elevated withdrawal rates. The maximum amount of eutectic is presented at the withdrawal rate of 100 μm/s (Fig. 1(c)). The reduced amount of eutectic can be detected at the lowest withdrawal rate of 10 μm/s (Fig. 1(a)) or the highest withdrawal rate of 500 μm/s (Fig. 1(f)). The γ–γ′ eutectic forms at the last stage of solidification due to the strong segregation of Al and Ta to the interdendritic regions. Therefore, the degree of segregation can be ranked by eutectic fractions in the as-cast microstructures. It suggests that the degree of segregation for the alloying elements increases initially and then decreases with increasing withdrawal rate.

3.3. Effects of withdrawal rate on the γ′ precipitates

As-cast microstructure of Ni-base superalloys consists of two basic phases: the γ matrix (disordered fcc structure) and strength-

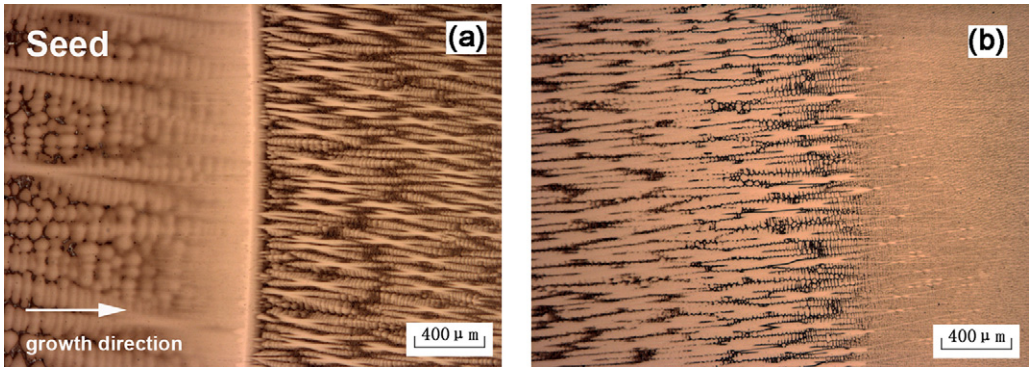

Fig. 3. (a) The incipient melting interface of the ⟨0 0 1⟩ oriented seed, which is produced by HRS method at the withdrawal rate of 100 μm/s and thermal gradient approximately 50 K/cm. (b) Quenched solid–liquid interface of alloy D, which is produced by LMC technique at the withdrawal rate of 100 μm/s and high thermal gradient approximately of 250 K/cm.

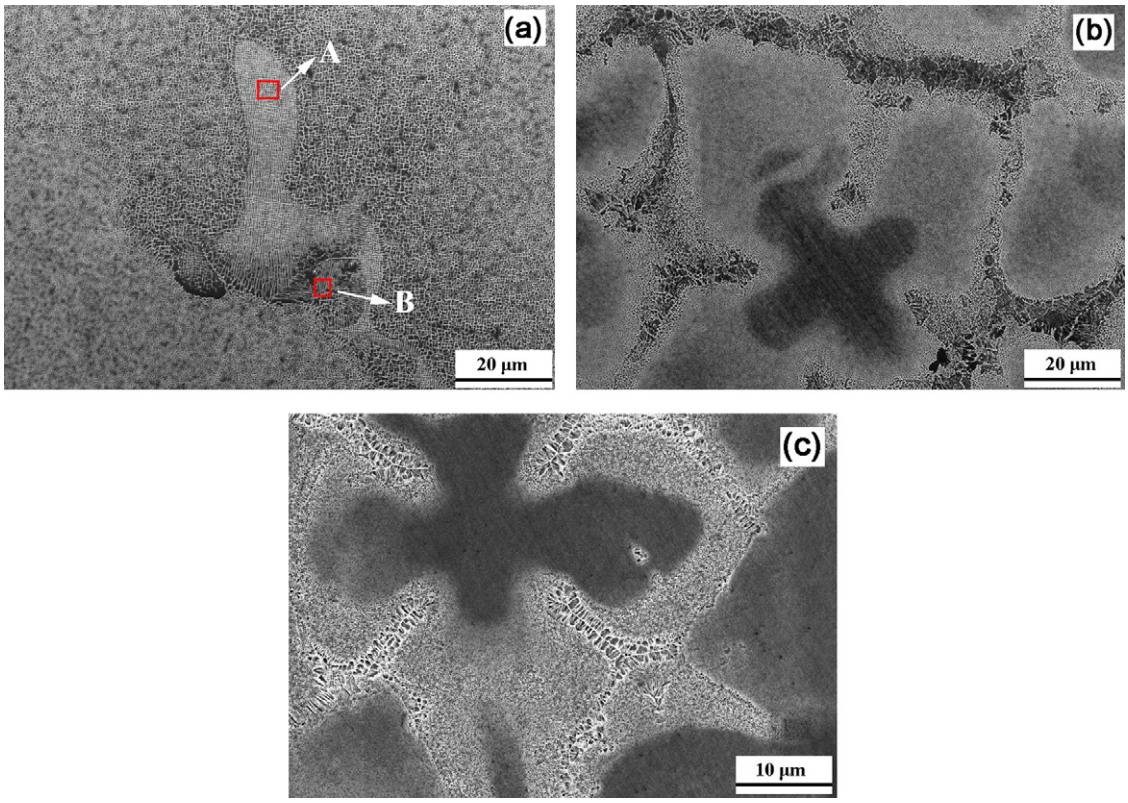

Fig. 4. SEM images of the γ–γ′ eutectic in the interdendritic regions of alloy D at various withdrawal rates. (a) 10 μm/s; (b) 100 μm/s; (c) 500 μm/s.

Table 2
Compositions (in wt.%) of γ–γ′ eutectic on the regions A and B (as shown in Fig. 4(a)) by using the energy-dispersive spectrometry (EDS) analysis.

	Element							
	Al	Cr	Co	Mo	Ru	Ta	W	Re
Region A	6.35	2.98	10.50	1.12	2.67	12.14	5.50	4.02
Region B	6.11	2.79	10.80	1.04	2.95	12.52	5.13	4.13
Alloy D	5.98	2.93	11.70	1.03	3.03	7.84	6.01	6.20

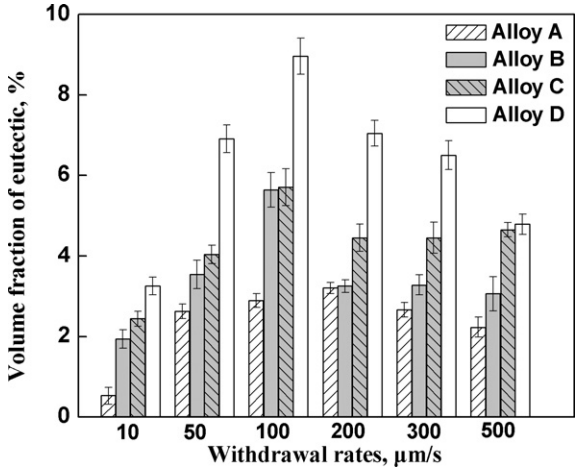

Fig. 5. Volume fraction of the γ–γ′ eutectic in the as-cast microstructures of alloys A, B, C and D with various withdrawal rates.

ening γ′ phase ($L1_2$ structure). During the cooling processing, γ′ phase coherently precipitates from the supersaturated γ-solid solution [18]. Fig. 6 shows the typical two-phases γ/γ′ microstructures of alloy D in the dendrite core (Fig. 6(a) and (c)) and interdendritic region (Fig. 6(b) and (d)). As well known, the driving force for the nucleation of γ′ precipitates is proportional to the supercooling degree (ΔT) and the supersaturation degree (ΔC). The increasing cooling rates lead to the growing degree of supercooling, and thus promote the nucleation of γ′ precipitates. Meanwhile, the increasing cooling rates reduce the time for the growth of γ′ precipitates. Therefore, the greatly refined γ′ precipitates can be detected at high withdrawal rate. When the withdrawal rate increases form 10 μm/s to 500 μm/s, the average size of γ′ precipitates in dendrite cores reduces from 0.23 μm to only about 0.03 μm. In addition, due to the segregation of γ′ forming elements (Al and Ta) to interdendritic regions, the size of γ′ precipitates in the interdendritic regions is much larger than that in the dendrite cores.

3.4. Effects of withdrawal rate on the segregation ratios

The dendrite segregation of the constituent elements in Ni-base single-crystal alloys are characterized by the segregation ratios, k', as given by

$$k' = \frac{C_{DC}}{C_{ID}} \tag{3}$$

where C_{DC} is the average concentration of the constituent element in the dendritic core, C_{ID} is that in the interdendritic region. $k' = 1$ indicates the homogeneously distributions of the constituent element. The segregation ratios greater or less than unity indicate

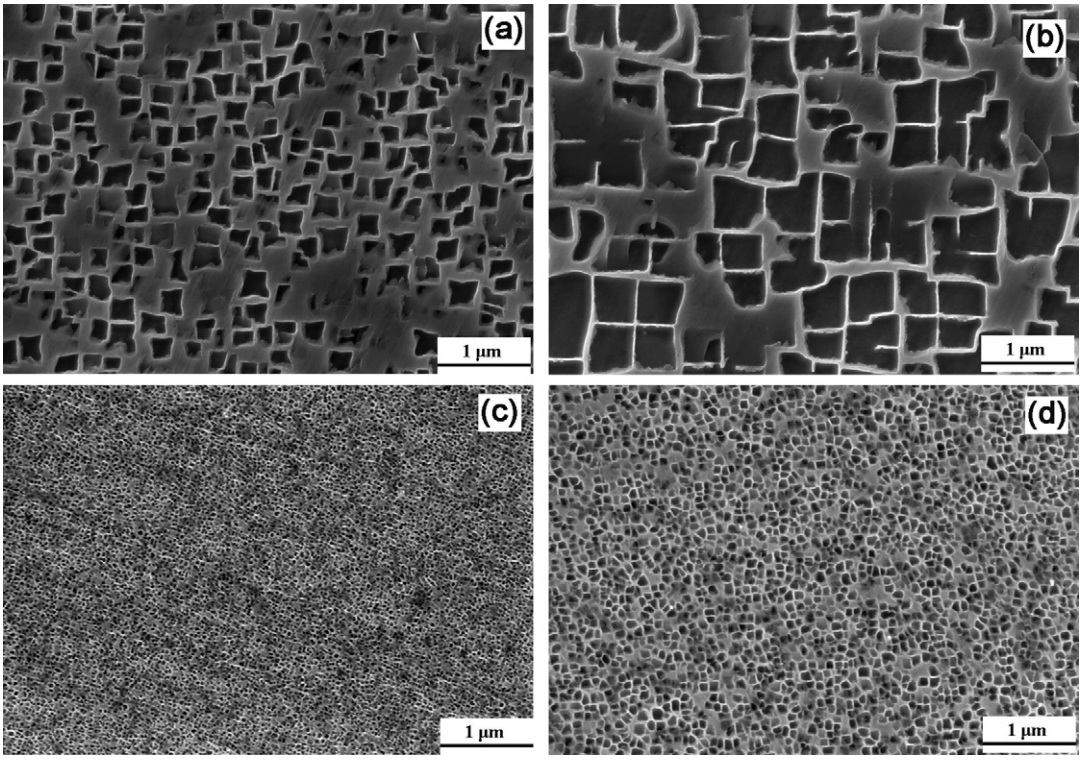

Fig. 6. SEM images of the γ′ phase in the dendrite core and interdendritic region of alloy D at different withdrawal rates. (a) Dendrite core, 10 μm/s; (b) Interdendritic region, 10 μm/s; (c) Dendrite core, 500 μm/s; (d) Interdendritic region, 500 μm/s.

that the corresponding element is partitioning preferentially to the dendrite core or interdendritic regions during solidification, respectively. The value of k' far away from unity indicates the more severe segregation.

The average EPMA compositions of dendrite cores and interdendritic regions for alloys A, B, C and D are recorded in Table 3. It can be clearly seen that Ta and Al strongly segregate to the interdendritic regions ($k' < 1$), whereas Re and W preferentially partition to the dendrite regions ($k' > 1$). The Co, Cr and Ru weakly segregate to the dendrite regions (k' slightly greater than 1).

The segregation ratios for the representative constituent elements (Re, W, Al and Ta) are plotted as a function of the withdrawal rate (Fig. 7). It is found that the values of k'_{Re} and k'_{W} increase initially and then decrease with increasing withdrawal rates (Fig. 7(a) and (b)). However, the values of k'_{Ta} and k'_{Al} decrease initially and then increase with increasing withdrawal rates (Fig. 7(c) and (d)). Therefore, the degree of segregation increases initially and then decreases with increasing withdrawal rate.

The influences of elevated withdrawal rate on the segregation behavior for the constituent elements can be greatly attributed to the homogeneous back-diffusion in the solidified solid. For solid back-diffusion, two factors need to be considered: the diffusion time ($\Delta T/GV$) and the diffusion distance (approximately equal to $\lambda_1/2$). At low withdrawal rate, the reduction in homogenous diffusion time plays the leading role, resulting in the increased degree of segregation. However, at higher withdrawal rates, the diffusion distance ($\lambda_1/2$) reduces significantly due to the greatly refined dendritic structures under high thermal gradient. The reduction of diffusion distance is the predominant factor to decrease the degree of segregation. Therefore, the degree of segregation for the constituent elements, particularly for Re, W, Ta and Al, increase initially and then decrease with increasing withdrawal rates.

As mentioned previously, Wilson et al. reported that increasing withdrawal rate leads to the more severe segregation of Ti, Ta and Re for the commercial superalloy CMSX-10 [19]. However, it should be noted that the investigation considered a relative low thermal gradient of approximately 15–20 K/cm. In this investigation, the dendritic structures are significantly refined under a high thermal gradient of approximately 250 K/cm. The obviously reduced segregation can be detected when withdrawal rate greater than 100 μm/s. The segregation of Re and W are difficult to be eliminated even by the complicated solution heat treatments [7,20]. Therefore, the greatly refined dendritic structures with low degree of segregation are beneficial for reducing the time for heat treatments and improving the mechanical properties.

3.5. Effects of Re and Ru on the segregation ratios

The segregation ratios of the constituent elements (e.g. Al, Ta, W, Re etc.) for alloys A, B, C and D at the withdrawal rate of 100 μm/s are shown in Table 3. The compositions of alloys A and C mainly vary in Re content. As the Re content is increased, the k' for Al and Ta decrease, indicating the degree of segregation for Al and Ta increase with Re addition. Compared with the k' of Re and W for alloys A (3 wt.% Re) and C (6 wt.% Re), it is found that Re additions increase the tendency of segregation for Re and W.

Alloys C and D have the similar contents of Re, but alloy D has additional Ru (3 wt.%). With increasing Ru addition, the tendency for Al and Ta segregation to interdendritic region increases. Compared with the k' of Re and W for alloys C and D, it is found that the Ru decrease the degree of segregation for Re and W to the dendrite core. However, the segregation ratios of Re are also influenced by elevated withdrawal rate. As shown in Fig. 7(a), the k' of Re for alloys C and D are close to each other, and change in a similar fashion with withdrawal rate, indicating the Ru has slight influences on the segregation behavior of Re.

Fig. 8 shows the transverse cross sections of the experimental alloys A, B, C and D at the withdrawal rate of 10 μm/s, respectively. Quantitative results of the eutectic volume fraction have been provided in Fig. 5. From the results of alloys A, B, C and D, as the level

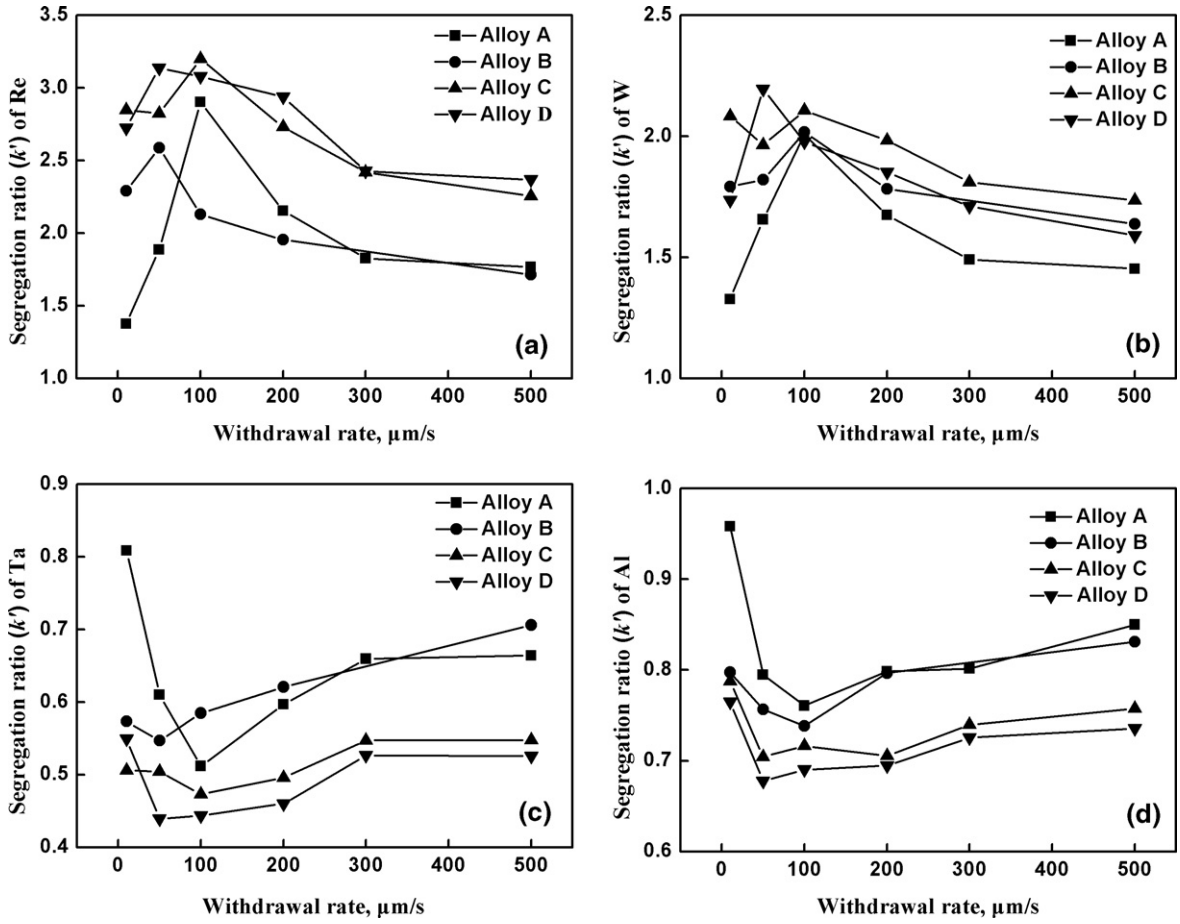

Fig. 7. Effects of withdrawal rates on the segregation ratios of the constituent elements. (a) Re; (b) W; (c) Ta; (d) Al.

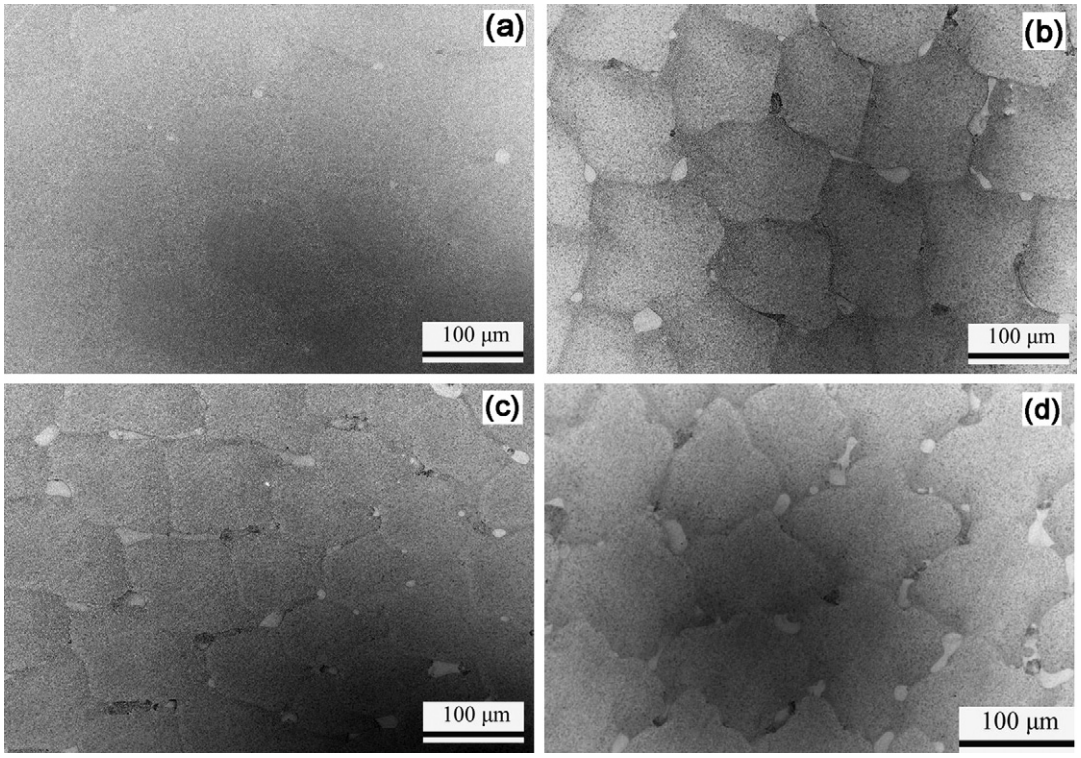

Fig. 8. Transverse cross sections of alloys A, B, C and D at the withdrawal rate of 10 μm/s. (a) Alloy A; (b) alloy B; (c) alloy C; (d) alloy D.

Table 3
Average EPMA compositions (wt.%) of the dendrite core and interdendritic regions, with corresponding segregation ratios, k', for alloys A, B, C and D at the withdrawal rate of 100 μm/s.

Alloy-region	Al	Ta	Cr	W	Co	Re	Ru
A							
Dendrite core	4.66	4.96	3.06	8.52	13.54	3.65	
Interdendritic region	6.12	9.69	2.93	4.24	11.93	1.26	
B							
Dendrite core	5.43	4.62	3.12	8.39	13.72	6.99	
Interdendritic region	7.13	9.24	2.83	4.35	12.12	3.03	
C							
Dendrite core	5.40	4.70	3.01	8.37	13.48	7.10	
Interdendritic region	7.54	9.93	2.64	3.97	11.42	2.22	
D							
Dendrite core	5.23	3.56	3.08	8.53	12.92	8.82	3.04
Interdendritic region	7.57	8.03	2.68	4.31	11.47	2.86	2.96
Segregation ratios							
A	0.76	0.51	1.04	2.01	1.13	2.90	
B	0.76	0.50	1.10	1.93	1.13	2.31	
C	0.72	0.47	1.14	2.21	1.18	3.20	
D	0.69	0.44	1.15	1.98	1.13	3.08	1.03

of Re and Ru is increased, the eutectic phase fraction rises significantly. The maximum fraction of eutectic can be detected in alloy D, which has the highest contents of Re and Ru, indicating the Re and Ru increase the segregation of Al and Ta.

4. Conclusions

Four Ni-base single-crystal alloys with varied contents of Re and Ru are investigated with the high thermal gradient directional solidification technique. The following conclusions can be drawn from this work:

(1) Under high thermal gradient, the dendritic structures are significantly refined with increasing withdrawal rates. The corresponding primary dendritic arm spacing reduces to only about 45 μm at the withdrawal rate of 500 μm/s. In addition, the γ′ precipitates are greatly refined with the elevated withdrawal rates.
(2) The degree of segregation for the constituent elements (e.g. Al, Ta, W and Re) increases initially and then apparently decreases with increasing withdrawal rates. The reduced segregation at high withdrawal rate can be greatly attributed to the refined dendritic structures.
(3) The Re and Ru additions increase the eutectic fractions and the degree of segregation for Al and Ta. The Ru slightly segregates to the dendrite region. The addition of Ru does not have obvious influence on the segregation of Re.

Acknowledgements

The authors would gratefully acknowledge the financial support from National Natural Science Foundation of China (Grant No. 50931004, No. 50827102, and No. 50771081), National Basic Research Program of China (Grant No. 2010CB631202 and No. 2011CB610406), National High Technology Research and Development Program (Grant No. 2007AA03Z552) and the fund of the State Key Laboratory of Solidification Processing in NWPU.

References

[1] S. Tin, T.M. Pollock, J. Propul. Power 22 (2006) 361–374.
[2] C.T. Liu, J. Ma, X.F. Sun, J. Alloys Compd. 491 (2010) 522–526.
[3] K. Zhao, Y.H. Ma, L.H. Lou, J. Alloys Compd. 475 (2009) 648–651.
[4] A. Heckl, R. Rettig, R.F. Singer, Metall. Mater. Trans. 41A (2010) 202–211.
[5] L. Zheng, S.S. Li, C.B. Xiao, D.Z. Tang, C.Q. Gu, Key Eng. Mater. 353–358 (2007) 507–510.
[6] Q. Feng, L.J. Carroll, T.M. Pollock, Metall. Mater. Trans. 37A (2006) 1949–1962.
[7] S.R. Hegde, R.M. Kearsey, J.C. Beddoes, Mater. Sci. Eng. A 527 (2010) 5528–5538.
[8] F. Long, Y.S. Yoo, C.Y. Jo, S.M. Seo, H.W. Jeong, Y.S. Song, T. Jin, Z.Q. Hu, J. Alloys Compd. 478 (2009) 181–187.
[9] M. Konter, E. Kats, N. Hofmann, in: T.M. Pollock, et al. (Eds.), Superalloys 2000, TMS, Warrendale, PA, 2000, pp. 189–200.
[10] Y.G. Nakagawa, Y. Ohtomo, Y. Sajga, in: J.K. Tien, et al. (Eds.), Superalloys 1980, AMS, Metals Park, OH, 1980, pp. 267–274.
[11] C. Wang, J. Zhang, L. Liu, H. Fu, J. Alloys Compd. 508 (2010) 440–445.
[12] X.W. Hu, S.M. Li, W.J. Chen, S.F. Gao, L. Liu, H.Z. Fu, J. Alloys Compd. 501 (2010) 110–114.
[13] L. Liu, T.W. Huang, M. Qu, G. Liu, J. Zhang, H.Z. Fu, J. Mater. Process. Technol. 210 (2010) 159–165.
[14] W. Kurz, D.J. Fisher, Fundamentals of Solidification, Trans Tech Publications, Enfield, 1998, pp. 85–88.
[15] X.W. Hu, S.M. Li, W.J. Chen, S.F. Gao, L. Liu, H.Z. Fu, J. Alloys Compd. 493 (2010) 112–116.
[16] X.F. Ding, J.P. Lin, H. Qi, L.Q. Zhang, X.P. Song, G.L. Chen, J. Alloys Compd. 509 (2011) 4041–4046.
[17] J.D. Hunt, Solidification and Casting of Metals, The Metals Society, London, 1979, pp. 3–9.
[18] A. Picasso, A. Somoza, A. Tolley, J. Alloys Compd. 479 (2009) 129–133.
[19] B.C. Wilson, E.R. Cutler, G.E. Fuchs, Mater. Sci. Eng. A 479 (2008) 356–364.
[20] Q. Zeng, S.W. Ma, Y.R. Zheng, S.Z. Liu, T. Zhai, J. Alloys Compd. 480 (2009) 987–990.